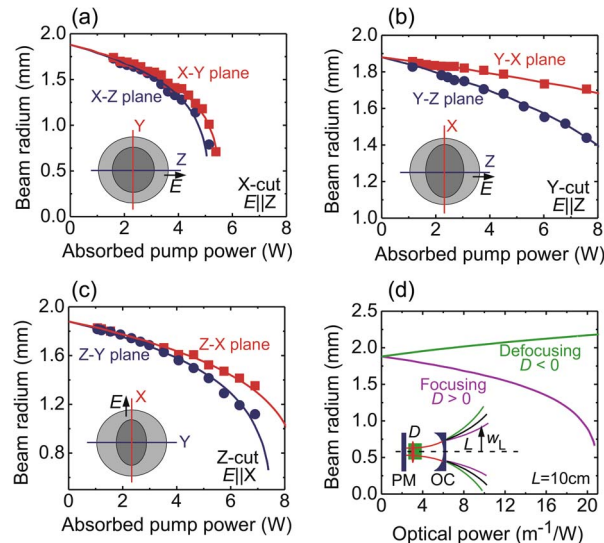


Thermal Lensing and Multiwatt Microchip Laser Operation of Yb:YCOB Crystals

Volume 8, Number 3, June 2016

Pavel Loiko
 Josep Maria Serres
 Xavier Mateos
 Haohai Yu
 Huaijin Zhang
 Junhai Liu
 Konstantin Yumashev
 Uwe Griebner
 Valentin Petrov
 Magdalena Aguiló
 Francesc Díaz



DOI: 10.1109/JPHOT.2016.2555584
 1943-0655 © 2016 IEEE

Thermal Lensing and Multiwatt Microchip Laser Operation of Yb:YCOB Crystals

Pavel Loiko,^{1,2} Josep Maria Serres,² Xavier Mateos,^{2,3} Haohai Yu,⁴
Huajin Zhang,⁴ Junhai Liu,⁵ Konstantin Yumashev,¹ Uwe Griebner,³
Valentin Petrov,³ Magdalena Aguiló,² and Francesc Díaz²

¹Center for Optical Materials and Technologies, Belarusian National Technical University,
220013 Minsk, Belarus

²Física i Cristal·lografia de Materials i Nanomaterials (FiCMA-FiCNA),
Universitat Rovira i Virgili (URV), 43007 Tarragona, Spain

³Max Born Institute for Nonlinear Optics and Short Pulse Spectroscopy, 12489 Berlin, Germany

⁴State Key Laboratory of Crystal Materials, Shandong University, Jinan 250100, China

⁵College of Physics, Qingdao University, Qingdao 266071, China

DOI: 10.1109/JPHOT.2016.2555584

1943-0655 © 2016 IEEE. Translations and content mining are permitted for academic research only.

Personal use is also permitted, but republication/redistribution requires IEEE permission.

See http://www.ieee.org/publications_standards/publications/rights/index.html for more information.

Manuscript received March 2, 2016; revised March 28, 2016; accepted March 30, 2016. Date of publication April 20, 2016; date of current version April 29, 2016. This work was supported by the Spanish Government under Project MAT2013-47395-C4-4-R and Project TEC2014-55948-R and by the Generalitat de Catalunya under Project 2014SGR1358. F. D. acknowledges additional support through the Catalan Institution for Research and Advanced Studies (ICREA) academia award 2010ICREA-02 for excellence in research. This work is part of a project that has received funding from the European Union's Horizon 2020 research and innovation programme under the Marie Skłodowska-Curie Grant agreement 657630. Corresponding author: X. Mateos (e-mail: xavier.mateos@urv.cat; mateos@mbi-berlin.de).

Abstract: Thermal lensing is studied in monoclinic Yb:Ca₄YO(BO₃)₃ (Yb: YCOB) oxoborate crystals cut along the optical indicatrix axes. For all orientations, the thermal lens is positive. In the Z-cut crystal, the sensitivity factors of the thermal lens are $M_{Z-X} = 2.4$ and $M_{Z-Y} = 2.8 \text{ m}^{-1}/\text{W}$ (for $E \parallel X$), and the astigmatism degree is as low as $S/M = 14\%$. The positive thermal lens in Yb:YCOB is related to the large thermal expansion and strong photoelastic effect. Microchip lasers are realized with 3-mm-long X, Y, and Z-cut 15 at.% Yb:YCOB crystals. With a Z-cut crystal, maximum output power of 8.35 W is achieved at ~1040 nm with slope efficiency of 70%. Using various crystal cuts and output coupler transmissions, multiwatt emission in the spectral range of 1033–1091 nm is demonstrated.

Index Terms: Diode-pumped lasers, microchip, thermal lensing, oxoborates.

1. Introduction

The monoclinic oxoborates Ca₄REO(BO₃)₃, where RE = Y or Gd (shortly denoted as YCOB and GdCOB, respectively), are promising laser host materials for doping with Yb³⁺ ions [1]. Yb-doped oxoborates combine the advantages of the Yb³⁺ ion arising from its simple energy scheme, i.e., relatively low thermal load, absence of parasitic excited-state absorption and up-conversion processes and high achievable laser efficiency, with broad and intense absorption and emission bands exhibiting strong polarization-anisotropy, as well as relatively long lifetime of the upper laser level (~2.6 ms) [2], [3]. Yb:YCOB and GdCOB can be efficiently pumped into the zero-line of Yb³⁺ with maximum absorption cross-section, $\sigma_{\text{abs}} \sim 1 \times 10^{-20} \text{ cm}^2$ at 976 nm [6] by commercial InGaAs laser diodes [4], [5]. The oxoborate hosts and YCOB in particular can also incorporate

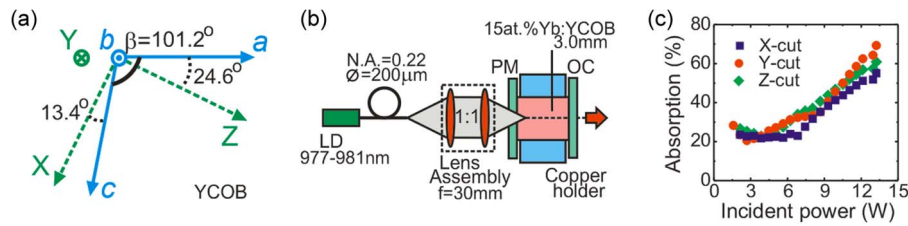


Fig. 1. (a) Orientation of the optical indicatrix axes (X , Y , Z) with respect to the crystallographic frame (a , b , c) of YCOB. (b) Scheme of the Yb:YCOB microchip laser setup: LD—laser diode, PM—pump mirror, and OC—output coupler. (c) Double-pass absorption of the different Yb:YCOB laser samples versus incident power (unpolarized pump).

high Yb^{3+} concentrations (up to 27 at.% for GdCOB and ~50 at.% for YCOB [5], [7]), thus providing laser compactness. YCOB and GdCOB melt congruently so they can be pulled directly from the melt which enables the growth of large-volume crystals with good optical quality [8], [9]. This is not the case for the isostructural passive hosts ScCOB, LaCOB and LuCOB or for the stoichiometric YbCOB crystal [7]. As a result, efficient continuous-wave (CW) [10], [11], passively Q -switched [12], [13] and mode-locked [14], [15] Yb oxoborate lasers have been realized to date. The thin-disk geometry has also been exploited for Yb:YCOB crystals [16].

The non-centrosymmetric YCOB and GdCOB crystals show good nonlinear properties [9], [17], [18] and are of practical interest for second-harmonic generation including self-frequency doubling [1], [13], [19] and chirped pulse optical parametric amplification [20].

A microchip laser contains a gain material placed in a plano-plano cavity without air gaps [21]. This laser design provides low losses and high efficiency in a robust, compact set-up and is insensitive to misalignment. The active material for a microchip laser should have high absorption and emission cross-sections and/or high available doping levels together with good thermal and thermo-mechanical properties. The key parameter that determines the feasibility of the material for microchip operation is the sign of the thermal lens. Positive (focusing) lens can provide stabilization of the laser mode in a plane-parallel resonator [22]. Positive thermal lens was measured for oxoborates for some particular crystal cuts [23]. From this point of view, Yb:YCOB and Yb:GdCOB seems to be good candidates for microchip lasers. However, to date, their potential in microlasers has not been fully exploited. We are aware of only one report on such microchip lasers [5] where both crystals generated a maximum output power of ~300 mW in the CW regime with a slope efficiency of 79%.

In the present work, our goal was to perform a comparative study of the parameters of the thermal lens in Yb:YCOB crystals cut along the principal optical directions and to realize Yb:YCOB microchip lasers delivering multi-watt-level output.

2. Experimental

The Yb:YCOB crystal was grown by the Czochralski method. It was doped with 15 at.% Yb ($N_{\text{Yb}} = 6.9 \times 10^{20}$ at/cm³). YCOB is a monoclinic crystal with structure belonging to the non-centrosymmetric space group Cm (the lattice parameters are $a = 8.046$ Å, $b = 15.959$ Å, $c = 3.517$ Å and $\beta = 101.2^\circ$) [1]. Each Y^{3+} ion is surrounded by six O^{2-} anions forming a distorted octahedron. Due to the relatively large Y^{3+} - Y^{3+} ion separation (the shortest distance is 3.517 Å) and closeness of ionic radii of the VI-fold oxygen-coordinated Y^{3+} (0.90 Å) and Yb^{3+} (0.868 Å), high doping levels are easily achievable in Yb:YCOB. YCOB is an optically biaxial host crystal. Its optical properties are described in the frame of the optical indicatrix [18], with the three mutually orthogonal principal axes X , Y , and Z (the corresponding refractive indices follow the relation $n_X < n_Y < n_Z$). The Y -axis is parallel to the $-b$ axis, while the X and Z axes are located in the $a-c$ plane ($a^{\wedge}Z = 24.6^\circ$ and $c^{\wedge}X = 13.4^\circ$) [18], Fig. 1(a).

For the study of thermal lensing and microchip laser properties of Yb:YCOB, three crystals with identical dimensions $3 \times 3 \times 3$ mm³ were cut for light propagation along the X , Y , and Z

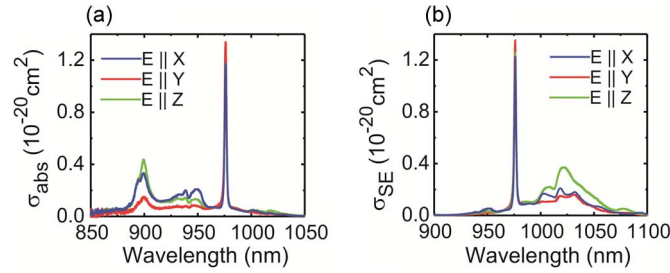


Fig. 2. Absorption σ_{abs} (a) and stimulated emission σ_{SE} (b) cross-sectional spectra for the 15-at.% Yb:YCOB crystal for the principal light polarizations, $E \parallel X, Y,$ and Z .

axes. Their input and output faces were polished to laser quality and remained uncoated. The crystals, wrapped with Indium foil to improve the thermal contact, were mounted in a copper holder and water-cooled at 12 °C.

The laser cavity for microchip experiments consisted of a flat pump mirror (PM) that was AR coated for 0.9–1.0 μm and HR coated for 1.02–1.20 μm , and a flat output coupler (OC) with transmission $T_{\text{OC}} = 1\%, 5\%$ or 10% at the laser wavelength, Fig. 1(b). Both PM and OC were in contact with the crystal faces, so that the geometrical cavity length was 3.0 mm. The pump source was a fiber-coupled InGaAs laser diode (N.A. = 0.22, fiber core diameter: 200 μm) emitting up to 25 W at $\sim 975, \dots, 977$ nm depending on the diode current level. A lens assembly with imaging ratio 1:1 and focal length of 30 mm provided a pump spot radius of $w_p = 100$ μm in the crystal. The confocal parameter for the pump beam $2Z_R$ was 3.0 mm ($M^2 \sim 20$). The pump radiation was unpolarized. The crystal was pumped in a double pass configuration due to the partial reflection of the OC at the pump wavelength.

The spectroscopic properties of the 15 at.% Yb:YCOB crystal were characterized in order to assist the interpretation of the absorption and emission characteristics of the lasers. The absorption spectra were measured with polarized light (using a Glan-Taylor polarizer) with a Varian CARY-5000 spectrophotometer in the 850–1100 nm spectral range with a spectral bandwidth (SBW) of 0.05 nm. The absorption cross-sections were determined from the absorption coefficient, $\sigma_{\text{abs}} = \alpha/N_{\text{Yb}}$, Fig. 2(a). The total absorption of the Yb:YCOB crystals amounted to 20, \dots , 70% depending on the diode current level due to a shift of its wavelength, Fig. 1(c). A relatively narrow zero-phonon-line absorption peak of Yb^{3+} ions is found in YCOB. In particular, λ_{ZL} is 976.2 nm and the full width at half maximum (FWHM) of this peak is only 2.1 nm, Fig. 2(a).

Stimulated-emission (SE) cross-sections σ_{SE} for Yb:YCOB were derived using the reciprocity method, which requires the knowledge of the absorption spectrum $\sigma_{\text{abs}}^i(\lambda)$ and the Stark splitting of the two multiplets $\{E_k^m\}$ [24]

$$\sigma_{\text{SE}}^i(\lambda) = \sigma_{\text{abs}}^i(\lambda) \frac{Z_1}{Z_2} \exp\left(-\frac{hc/\lambda - E_{\text{ZL}}}{kT}\right) \quad (1)$$

where i stands for the light polarization; $i = X, Y,$ or Z ; E_{ZL} is the energy difference between the lowest Stark sub-levels of the two multiplets (zero-phonon line); k is the Boltzmann constant; T is the crystal temperature (room temperature); and Z_m are the partition functions lower ($m = 1$) and upper ($m = 2$) manifolds

$$Z_m = \sum_k g_k^m \exp(-E_k^m/kT). \quad (2)$$

Here, g_k^m is the degeneration of the sub-level with the number k and energy E_k^m measured from the lower sublevel of the multiplet. The energies of the Stark sub-levels for the ${}^2F_{7/2}$ and ${}^2F_{5/2}$ multiplets of Yb^{3+} in YCOB can be found elsewhere [4]. The results on SE cross-sections for

TABLE 1

Anisotropy of thermal coefficients of the optical path for YCOB crystals at $\sim 1 \mu\text{m}$ [27]

Crystal	Orientation	TCOP*, 10^{-6}K^{-1}		
		$E \parallel X$	$E \parallel Y$	$E \parallel Z$
YCOB	X-cut	–	+4.5	+5.9
	Y-cut	+0.6	–	–0.8
	Z-cut	+2.9	+0.5	–

*TCOP = $dn/dT + (n-1)\alpha$

15 at.% Yb:YCOB are shown in Fig. 2(b). They will be used for the calculation of the gain cross-sections.

For the thermal lens characterization, a hemispherical cavity was used having an OC with a radius of curvature $R = 50 \text{ mm}$ and $T_{OC} = 5\%$. The laser mode was TEM_{00} in this case, with $M^2 < 1.05$. The radius of the output beam from this laser was determined along the directions of the optical indicatrix axes at different pump levels by the ISO-standard moving knife-edge method [25]. The optical (refractive) power of the lens ($D = 1/f$, f denotes focal length) was derived from the ABCD-modeling [26]. This method has larger errors to determine the optical power ($\sim 10\text{--}15\%$) as compared with the approach based on Shack-Hartmann sensor, which was used previously for the study of the thermal lens in Yb-doped oxoborates [23]. However, its realization is much easier. The main assumptions for our model are the following: i) thermal lens described as an ideal thin astigmatic lens located in the center of the laser crystal; ii) high-order thermo-optic aberrations are neglected; iii) the laser beams are considered as elliptic Gaussian ones with M^2 approaching unity; iv) the polarization of the laser beam is linear.

3. Results and Discussion

In a recent study of the thermo-optic properties of YCOB crystal, it was shown that its thermo-optic coefficients (TOC), dn/dT , are negative, $dn_X/dT = -1.2$, $dn_Y/dT = -3.7$ and $dn_Z/dT = -2.5 \times 10^{-6} \text{K}^{-1}$ (at $\sim 1 \mu\text{m}$) [27]. On the other hand, the thermal expansion coefficients (α) for this crystal are relatively large and exhibit strong anisotropy, $\alpha_X = 12.0$, $\alpha_Y = 2.6$, $\alpha_Z = 6.2 \times 10^{-6} \text{K}^{-1}$ [27]. This determines the possibility of both positive and negative overall thermal variation of the optical path length for this material, depending on the crystal cut and light polarization, see Table 1, where the values of the thermal coefficient of the optical path (TCOP) are listed. TCOP represents the variation of the optical path length (OPL) for light rays passing through an uniformly heated stress-free optical material [28]. Although TCOP includes the contributions of dn/dT and thermal expansion, it cannot be directly used for the description of thermal lens as it does not account for the thermal stresses and the non-uniform temperature field in the diode-pumped crystal. However, TCOP is useful for the prediction of the sign of the thermal lens and its mean refraction.

In the present work, direct measurements of the parameters of the thermal lens were performed for the X, Y, and Z-cut Yb:YCOB crystals for the polarization state naturally selected by the anisotropy of the gain [2], [6], i.e., $E \parallel Z$ for the X-cut and Y-cut crystals and $E \parallel X$ for the Z-cut one. The laser wavelength was $\sim 1050 \text{ nm}$ for the X-cut and Y-cut crystals and 1038 nm for the Z-cut one.

The measured radii of the output laser mode for the X-, Y-, and Z-cut Yb:YCOB lasers are shown in Fig. 3(a)–(c). According to the ABCD-modelling, Fig. 3(d), positive (focusing, with $D > 0$) thermal lens in such a laser results in the beam compression in the far-field while negative (diverging, with $D < 0$) thermal lens will lead to the beam expansion. This allows one to determine unambiguously the sign of the lens. For all three crystal cut, the laser beam is compressed along the two principal directions. As a result, the beam becomes elliptic with the minor semiaxis corresponding to the stronger lens (larger D). Larger beam ellipticity is observed for Y-cut crystal, while for X- and Z-cut ones, it is much weaker. This indicates that the thermal

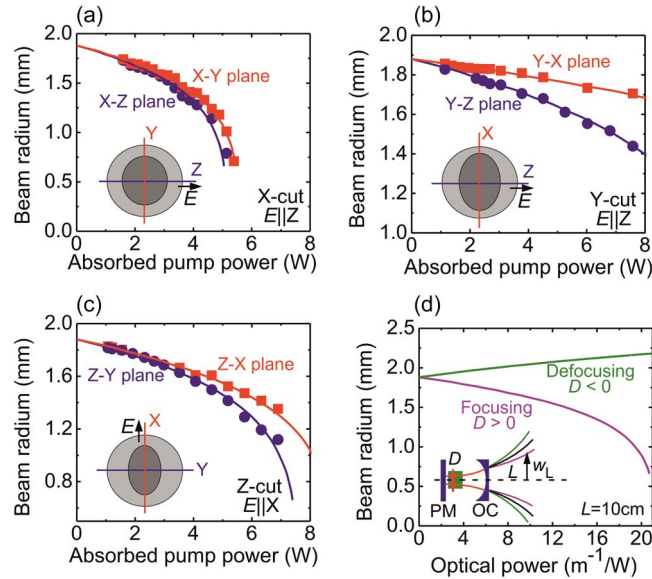


Fig. 3. Radii of the output laser beam versus the absorbed pump power for (a) X-cut, (b) Y-cut, and (c) Z-cut Yb:YCOB crystals: hemispherical cavity ($R_{OC} = 50$ mm). The symbols are their fitting with the ABCD method, and the distance from the OC is 10 cm. (Insets) Scheme of the beam distortion (light-gray circle—beam close to the laser threshold; grey ellipse—at high pump power; E—laser polarization; red and blue lines—principal meridional planes). (d) Calculated dependence of the beam radius on the optical power D of positive and negative thermal lenses for Yb:YCOB hemispherical laser [(Inset)—scheme of the experiment].

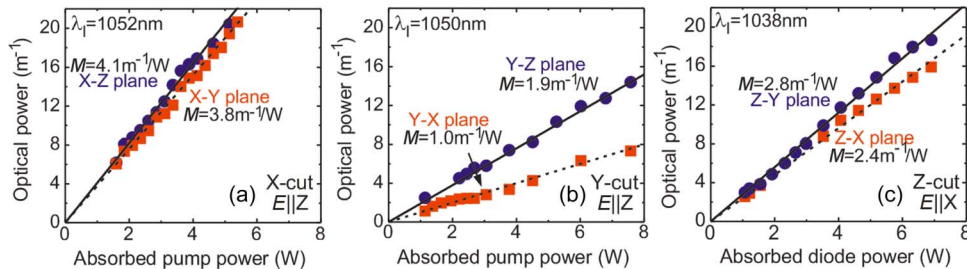


Fig. 4. Optical power of the thermal lens versus absorbed diode power for (a) X-cut, (b) Y-cut, and (c) Z-cut Yb:YCOB crystals. Symbols are the experimental data, and lines are their fitting for the calculation of the sensitivity factors ($M = dD/dP_{abs}$).

lens is positive in all X-, Y-, and Z-cut Yb:YCOB crystals. In Fig. 3(a)–(c), the curves are from the modelling of the beam distortion with the ABCD-method. One can see that they fit accurately the experimental data.

The dependence of the optical power of the thermal lens D on the absorbed diode power P_{abs} is shown in Fig. 4 for the three crystal cuts. Its slope is expressed by a sensitivity factor, $M = dD/dP_{abs}$ [28]. The error in its determination was ± 0.3 m⁻¹/W. The thermal lens is found to be positive for X-, Y-, and Z-cut Yb:YCOB crystals. The X-cut crystal exhibits the strongest lens, $M_{X-Z} = 4.1$ and $M_{X-Y} = 3.8$ m⁻¹/W (for $E \parallel Z$). Here the notations X–Z and X–Y refer to the meridional planes of the lens. This is in agreement with the maximum TCOP value (5.9×10^{-6} K⁻¹) observed for the X-cut crystal and $E \parallel Z$, cf. Table 1. For the Y- and Z-cut crystals, the thermal lens is weaker, with the following M -factors: $M_{Y-X} = 1.0$ and $M_{Y-Z} = 1.9$ m⁻¹/W (Y-cut, for $E \parallel Z$) and $M_{Z-X} = 2.4$ and $M_{Z-Y} = 2.8$ m⁻¹/W (Z-cut, for $E \parallel X$). This is in

TABLE 2

Parameters of the thermal lens for Yb:YCOB crystals

Parameter	Crystal cut*		
	X-cut	Y-cut	Z-cut
Laser polarization	$E \parallel Z$	$E \parallel Z$	$E \parallel X$
Wavelength, nm	1052	1050	1038
Sensitivity factor M , m^{-1}/W	3.8 (X-Y)	1.0 (Y-X)	2.4 (Z-X)
	4.1 (X-Z)	1.9 (Y-Z)	2.8 (Z-Y)
Astigmatism degree S , m^{-1}/W	0.3	0.9	0.4
Astigmatism, S/M	7%	47%	14%
"Generalized" TOC χ , $10^{-6} K^{-1}$	6.4 (X-Y)	1.7 (Y-X)	4.8 (Z-X)
	6.9 (X-Z)	3.2 (Y-Z)	5.6 (Z-Y)
dn/dT , $10^{-6} K^{-1}$	-2.5	-2.5	-1.2
Photoelastic term** P_{PE} , $10^{-6} K^{-1}$	-1.7 (X-Y)	1.9 (Y-X)	1.1 (Z-X)
	-1.2 (X-Z)	3.4 (Y-Z)	1.9 (Z-Y)
End-bulging term Q_{dist} , $10^{-6} K^{-1}$	10.6	2.3	4.9

*Meridional planes of the lens are denoted in brackets, if applicable.

**Estimated as $P_{PE} = \chi - dn/dT - Q_{dist}$

agreement with the lower TCOP value for the Z-cut crystal ($2.9 \times 10^{-6} K^{-1}$). For the Y-cut crystal, however, slightly negative TCOP was deduced ($-0.8 \times 10^{-6} K^{-1}$). The reason for this discrepancy between the signs of the thermal lens and the TCOP will be explained below.

For all the three crystals, the M -factors in the two meridional planes (A and $B \equiv X, Y$ or Z) are different indicating that the thermal lens is astigmatic. The astigmatism degree, defined as $S = |M_A - M_B|$ is 0.3, 0.9, and 0.4 m^{-1}/W for X , Y , and Z -cut crystals, respectively. The astigmatism in laser crystals is often expressed with respect to the maximum refraction (maximum M value) in the form of S/M , which is useful to understand the laser beam ellipticity [28]. In the present case, the maximum astigmatism corresponds to the Y -cut (\mathbf{b} -cut) crystal (as $S/M = 47\%$) and it is substantially lower for the X -cut ($S/M = 7\%$) and Z -cut ($S/M = 14\%$) crystals. This situation is similar to the one observed previously in monoclinic Yb:KLu(WO₄)₂ crystals for which the larger astigmatism of the thermal lens also corresponded to the crystal cut along the \mathbf{b} -axis [26]. Consequently, stronger ellipticity of the laser beam is expected to occur for Y -cut Yb:YCOB. The parameters of the thermal lens for Yb:YCOB crystals are summarized in Table 2.

The thermal lens in a diode-pumped solid-state material is determined by three main factors [29]: (i) temperature dependence of the refractive index (expressed by dn/dT), photo-elastic effect (expressed by the P_{PE} term) and macroscopic bulging of the crystal end faces due to non-uniform thermal expansion (expressed by the Q_{dist} term, $Q_{dist} = (1 + \nu^*)(n - 1)\alpha$ where ν^* is the parameter showing the contribution of thermal expansion to the total axial strain [30], $\nu^* \approx \nu$ and ν is the Poisson ratio). The direction-averaged Poisson ratio of YCOB $\langle \nu \rangle = 0.29$ is determined in the present study from the previously reported compliances tensor [31]. The sum of these terms composes the "generalized" thermo-optic coefficient $\chi = dn/dT + P_{PE} + Q_{dist}$. The "Generalized" TOC represents the total variation of the OPL for light rays passing through the real pumped laser element, and it determines the M -factor of the thermal lens [29]

$$M = \frac{\eta_h}{2\pi w_p^2 \kappa} [dn/dT + P_{PE} + Q_{dist}] \quad (3)$$

where η_h is the fractional heat loading that can be estimated from the quantum defect, $\eta_h = 1 - (\lambda_p/\lambda_L)$, κ is the thermal conductivity ($\kappa_a = 1.83$, $\kappa_b = 1.72$, and $\kappa_c = 2.17$ W/mK [32]) and the factor of "2" accounts for the top-hat profile of the pump beam. From (3) and the measured M -factors, one can derive the χ values; see Table 1. Then, as the dn/dT coefficients of YCOB have been directly measured [27] and the Q_{dist} term can be directly calculated from the known material parameters, the photo-elastic term can be estimated as $P_{PE} = \chi - dn/dT - Q_{dist}$; see Table 2. For Yb:YCOB, P_{PE} can be either negative (for X -cut crystal) or positive (for Y and

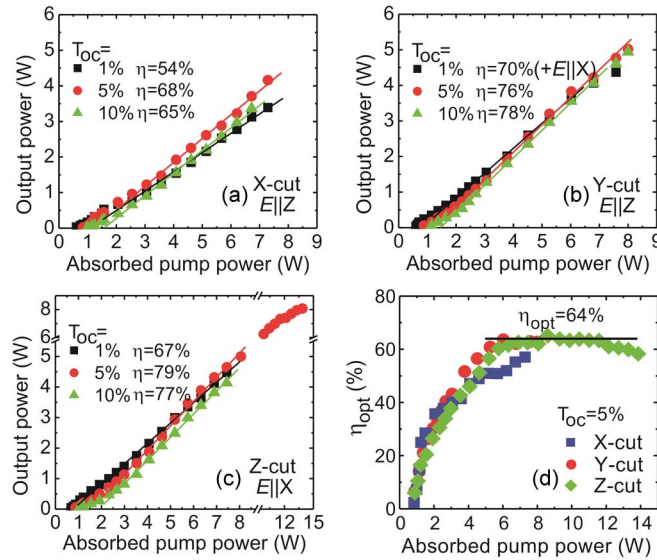


Fig. 5. Input–output dependences for (a) X-cut, (b) Y-cut, and (c) Z-cut Yb:YCOB microchip lasers. The symbols are the experimental data, and the lines are their fitting for the extraction of the slope efficiency (η). (d) Optical-to-optical efficiency η_{opt} for Yb:YCOB microchip lasers, $T_{OC} = 5\%$.

Z-cut crystals). Although its absolute value is relatively small, $< 2 \times 10^{-6} \text{ K}^{-1}$, it is comparable to the dn/dT and Q_{dist} terms, thus playing an important role in the formation of the positive lens for the Y-cut crystal. For the X- and Z-cut Yb:YCOB crystals, the positive sign of the thermal lens is mainly determined by the large thermal expansion (i.e., through the Q_{dist} term). The photo-elastic effect is responsible for the astigmatism of the thermal lens.

Previously, the thermal lens was measured for 15 at.% Yb-doped YCOB and GdCOB crystals using a Shack-Hartmann sensor [23], however, without consideration of its astigmatism. For the X-cut Yb:YCOB crystal, the M -factor was determined to be $5.6 \text{ m}^{-1}/\text{W}$ and for Y-cut Yb:GdCOB, $M = 2.5 \text{ m}^{-1}/\text{W}$ which is in agreement with our results.

As a consequence, although Yb:YCOB possesses negative thermo-optic coefficients, the combination of large thermal expansion and a strong photo-elastic effect determines the positive sign of the thermal lens for crystals cut along the principal optical directions. Therefore, X, Y, and Z-cut Yb:YCOB crystals are suitable for microchip laser operation because the positive thermal lens will provide stabilization of the laser mode in the plano-plano microchip cavity. Our calculations indicate that the radius of the laser mode in the Yb:YCOB microchips will be $w_l = 60 \pm 10 \text{ }\mu\text{m}$ for P_{abs} up to at least 15 W (see below).

Microchip laser operation was achieved with the X, Y, and Z-cut crystals. For all OCs, the laser output was linearly polarized and the polarization was naturally selected by the anisotropy of the gain. As already mentioned, for the X- and Y-cut crystals, it was $E \parallel Z$ and for the Z-cut crystal, it was $E \parallel X$. Only for the Y-cut Yb:YCOB crystal with specific loss adaptation ($T_{OC} = 1\%$), a coexistence of both possible polarization states $E \parallel X$ and $E \parallel Z$ was observed.

In the first microchip experiment, all three crystals were pumped up to $\sim 8 \text{ W}$ of absorbed diode power to avoid risk of thermal fracture. Within this pump range, the input-output dependences were clearly linear (see Fig. 5), indicating no detrimental influence of thermal effects. The Y- and Z-cut Yb:YCOB crystals showed very similar performance. For the Z-cut crystal, a maximum output power of 4.65 W was extracted at 1035, . . . , 1045 nm (multi-peak spectrum) with a slope efficiency η of 79% for $T_{OC} = 5\%$. The laser threshold was at $P_{abs} = 0.9 \text{ W}$. The optical-to-optical efficiency was 64%. At almost the same ($\eta = 77\%$) slope efficiency, with the 10% OC the laser oscillated at 1033, . . . , 1039 nm. For 1% OC, the slope efficiency was lower, 67%, and the laser emission was in the 1084–1090 nm range. The inferior performance of the

TABLE 3

Output characteristics^{*} of the Yb:YCOB microchip lasers

Crystal cut	Polariz.	T_{OC} , %	P_{th} , W	P_{out} , W	η , %	η_{opt} , %	λ_L , nm
X-cut	$E \parallel Z$	1	0.6	3.39	54	46	1055–1070, 1085–1091
		5	0.8	4.16	68	57	1043–1058
		10	1.0	3.37	65	50	1033–1042
Y-cut	$E \parallel Z$	1**	0.6	4.37	70	58	1056–1061, 1082–1090
		5	0.9	5.02	76	64	1042–1054
		10	1.1	4.94	78	61	1038–1050
Z-cut	$E \parallel X$	1	0.7	4.47	67	60	1084–1090
		5	0.9	4.65	79	64	1035–1045
		10	1.1	4.14	77	56	1033–1039

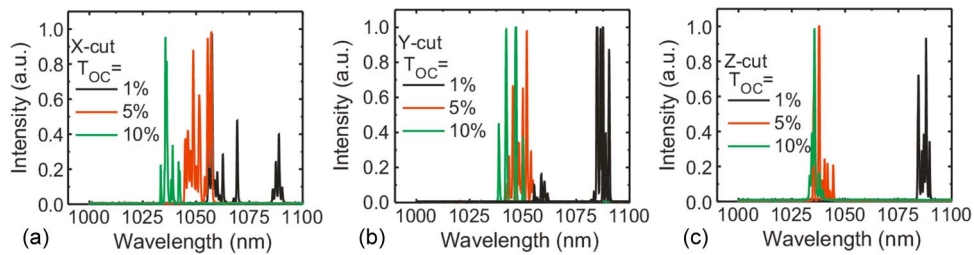
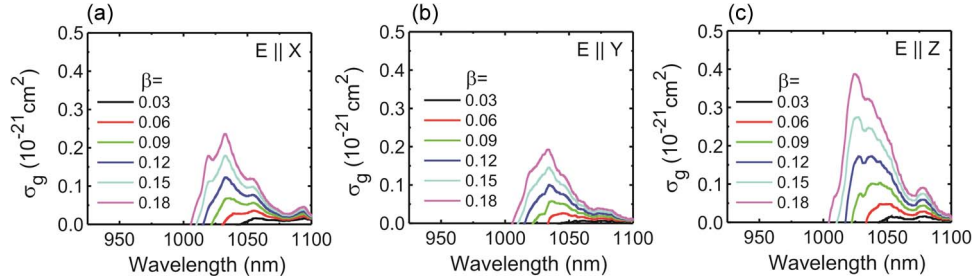
^{*} P_{th} – laser threshold, P_{out} – output power, η – slope efficiency, η_{opt} – optical-to-optical efficiency, λ_L – laser wavelength.^{**}Coexistence of two polarizations, $E \parallel X$ (dominant) and $E \parallel Y$.

Fig. 6. Laser emission spectra for (a) X-cut, (b) Y-cut, and (c) Z-cut Yb:YCOB microchip lasers. The absorbed pump power is 7 W.

Fig. 7. Calculated gain cross sections $\sigma_g = \beta\sigma_{SE} - (1 - \beta)\sigma_{abs}$ for the 15 at.% Yb:YCOB crystal for the principal light polarizations (a) $E \parallel X$, (b) $E \parallel Y$, and (c) $E \parallel Z$ at different inversion ratios β .

X-cut crystal is attributed to the stronger thermal lens, see Fig. 4(a). The output characteristics of the X, Y, and Z-cut Yb:YCOB microchip lasers are summarized in Table 3.

The laser emission spectra of the Yb:YCOB microchip lasers are presented in Fig. 6. All of them show multi-peak behavior typical for low-loss CW microchip lasers. With the increase of T_{OC} , the spectra experience a blue-shift in accordance with the gain spectral dependence [2], [6]. In order to explain the spectral properties of the laser emission from the Yb:YCOB lasers, we have plotted the gain cross-sections spectra ($\sigma_g = \beta\sigma_{SE} - (1 - \beta)\sigma_{abs}$) for the three principal light polarizations, $E \parallel X$, Y , and Z ; see Fig. 7. Here, β is the inversion ratio, $\beta = N_2/N_0$ where N_2 and N_0 are the number of ions excited in the upper laser level ($^2F_{5/2}$) and the overall number of ions, respectively. For very low $\beta < 0.05$, the gain cross-sections follow the relation $\sigma_g(Z) \approx \sigma_g(X) > \sigma_g(Y)$. This explains the possibility of the coexistence of $E \parallel X$ and Z oscillation states for Y-cut crystal at very low output coupling, as well as the generation of linearly polarized output for X-cut and Z-cut ones (at low T_{OC}). For $\beta > 0.05$ (larger T_{OC}), the following

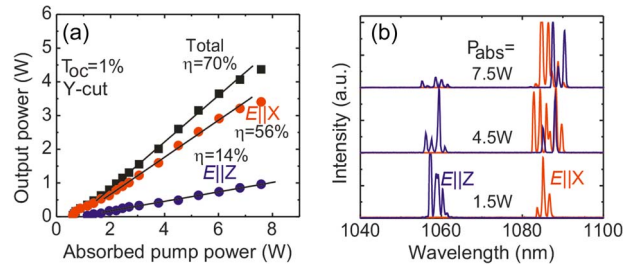


Fig. 8. Coexistence of $E \parallel X$ and $E \parallel Z$ polarization states for the Y-cut Yb:YCOB microchip laser with $T_{OC} = 1\%$: (a) output power versus absorbed pump power and (b) laser emission spectra at several absorbed power levels.

relation holds: $\sigma_g(Z) > \sigma_g(X) > \sigma_g(Y)$; therefore, so no conditions for coexistence of different polarization states is observed and thus Z-polarized light is generated in X-, and Y-cut Yb:YCOB lasers, and X-polarized light is generated in the Y-cut one.

With the increase of β , which corresponds to an increase of T_{OC} , the maxima in the gain spectra are shifted to shorter wavelengths. This is in agreement with the spectra of the laser emission, Fig. 6. In particular, for $E \parallel Z$ at low $\beta < 0.05$, the gain spectrum contains two broad bands centered at ~ 1.06 and $1.09 \mu\text{m}$. Indeed, for $T_{OC} = 1\%$, X-cut Yb:YCOB laser generates multi-peak emission at 1055–1070 and 1085–1091 nm corresponding to a nearly equal gain within these two local bands. For $E \parallel Z$, at higher β , one broad peak is formed in the gain spectrum, which is shifted from ~ 1.05 to $1.04 \mu\text{m}$ with the increase of the inversion ratio. Indeed, for $T_{OC} = 5\%$, the X-cut Yb:YCOB laser generates at 1043–1058 nm and for $T_{OC} = 10\%$, it operates at 1033–1042 nm.

The potential for further power scaling of the Yb:YCOB microchips was studied with the Z-cut crystal and $T_{OC} = 5\%$. In this case, a saturation of the output dependence was observed, Fig. 5(c). The maximum output power reached 8.35 W at $P_{abs} = 13.9$ W with $\eta = 70\%$ (calculated for the entire pump range) and an optical-to-optical efficiency of 59%. At higher P_{abs} , an abrupt drop of the laser output was observed.

By analyzing the data on laser thresholds and slope efficiencies (cf. Table 3) with the simple model of CW Yb laser (see details in [33]) and using the spectroscopic parameters presented in Fig. 2, we have estimated the round-trip internal losses for 3 mm-long 15 at.% Yb:YCOB as $L = 0.041 \pm 0.005$ (when averaged over the three crystal cuts, which were made from the same part of the grown bulk). This value is obtained by subtracting the contribution of Fresnel losses. The loss coefficient is then $\delta = 0.0068 \pm 0.0008 \text{ cm}^{-1}$ which is reasonably low and is determined mainly by the high doping level.

For the Y-cut Yb:YCOB crystal and $T_{OC} = 1\%$, the laser emission was polarized along the X- and Z-axes as mentioned above, Fig. 8. This behavior is due to i) low cavity loss of the microchip including low T_{OC} , ii) similar gain cross-sections in Yb:YCOB for these two polarizations, $\sigma_g(Z) \approx \sigma_g(X)$, at low inversion rates $\beta < 0.05$; see Fig. 7. No redistribution of the laser power between the two polarization states with the pump level (polarization-switching) was observed. The fraction of the output power for $E \parallel X$ was $\sim 80\%$. Such a coexistence is attributed typically to the anisotropy of the thermal lens properties for the two polarizations [34] which is not expected in the case of Yb:YCOB. Indeed, the thermal lens for $E \parallel Z$ is weak and positive ($\chi = 1.7, \dots, 3.2 \times 10^{-6} \text{ K}^{-1}$) and for $E \parallel X$ it will be very similar ($\text{TCOP} = 0.6 \times 10^{-6} \text{ K}^{-1}$, Table 1). The coexistence of the two orthogonal polarization states resulted in laser emission in two spectral ranges, 1056–1061 and 1082–1090 nm. This correlates well with the gain spectra for $E \parallel X$ and Z at low $\beta < 0.05$, Fig. 7. Both of them contain two broad local bands centered at ~ 1.06 and $1.09 \mu\text{m}$ corresponding to an almost equal gain.

The output beams for the X- and Z-cut Yb:YCOB microchip lasers corresponded to TEM_{00} mode with excellent circular profile and $M^2 < 1.05$ (measured at $P_{abs} = 7$ W), Fig. 9. This is attributed to the low astigmatism of the thermal lens for these crystal cuts. For the Y-cut crystal,

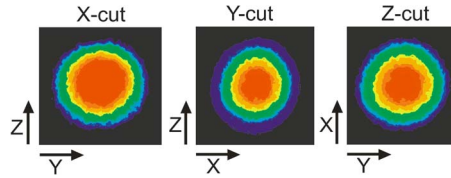


Fig. 9. Profiles of the output laser beam for X-cut, Y-cut, and Z-cut Yb:YCOB microchip lasers ($P_{\text{abs}} = 7$ W).

TABLE 4

CW oxoborate microchip lasers reported so far

Crystal	Output	Pump	P_{out} , mW	λ_L , nm	η , %	η_{opt} , %	Ref.
Nd:GdCOB	SHG	diode**	20	530	—	>2.5*	[35]
	SHG	Ti:Sa	43	530	—	>5*	
Nd:GdCOB	Fundamental	diode**	150	1060,1091	32	15	[36]
	SHG	diode**	22	545	—	2.2	
Er,Yb:YCOB	Fundamental	diode	100	1550	23	9	[37]
Yb:YCOB	Fundamental	diode	300	1050	67	27	[5]
Yb:GdCOB	Fundamental	diode	270	1050	79	25	[5]
Yb:YCOB	Fundamental	diode	8350	1035–1045	70	60	This work
			4650	1035–1045	79	64	This work

*Determined with respect to incident power.

**Polarized diode-pumping ($E \parallel Z$).

the output beam was slightly elliptic (as S is as high as 47%), and $M^2 < 1.1$. The M^2 factors were determined by an ISO-standard method fitting the beam divergence of a laser beam focused by a spherical lens [25]. The procedure was repeated in two orthogonal planes containing the optical indicatrix axes.

Previously, CW microchip laser operation was studied for Yb-doped YCOB and GdCOB crystals, Nd:GdCOB, and Er,Yb:YCOB. These results are listed in Table 4. The Nd-doped GdCOB was cut to satisfy the $oo - e$ type-I phase-matching condition for self-frequency doubling in the $X - Y$ plane ($\theta = 90^\circ$, $\varphi = 46^\circ$ at 1064.2 nm) [35], [36]. The maximum fundamental output power in [36] amounted to 150 mW at 1060 + 1091 nm ($E \parallel Z$), while 42 mW of green output power at 530 nm was measured. The slope efficiency for the fundamental output reached 32%. For the described crystal orientation in the $X - Y$ plane, the TCOP can be calculated as $dn_Z/dT + (n_Z - 1)\alpha_{X+46^\circ}$ where $\alpha_{X+46^\circ} \approx \alpha_X \cos^2 \varphi + \alpha_Y \sin^2 \varphi$, resulting in $3.9 \times 10^{-6} \text{ K}^{-1}$. Thus, positive thermal lens is expected for this crystal cut.

The 15 at.% Yb:GdCOB and 35 at.% Yb:YCOB microchips studied in [5] generated output powers as high as 300 mW (Yb:YCOB) while the slope efficiency with Yb: GdCOB reached $\eta = 79\%$. However, in [5], the orientation of the sample as well as the laser polarization were not specified. The present work represents the first study of microchip operation particularly with an oriented Yb:YCOB, which is relevant for this strongly anisotropic material. We present a substantial improvement of the previous results in terms of output power (> 8 W) keeping the very high slope efficiency (79% for output < 5 W and ~70% for the entire pump range). This is attributed to the selection of the optimal crystal orientation (Z-cut) with a weak and low-astigmatic thermal lens.

Monoclinic Yb:YCOB crystals provide better opportunities for power scaling as compared with monoclinic Yb:KLuW double tungstates which have been recently employed for microchip lasers [37] although the thermal conductivity of double tungstates is higher ($\kappa \approx 3 \text{ W/mK}$). Indeed, in [37], Yb:KLuW crystals of the same size and quality were studied in a similar set-up, and high risk of thermal fracture was detected for $P_{\text{abs}} > 10$ W. For Yb:YCOB, we have not observed fracture up to at least $P_{\text{abs}} \sim 15$ W. We refer this to the several degrees of anisotropy of the elastic properties of these materials.

4. Conclusion

We presented a detailed study of thermal lensing in Yb:YCOB crystals cut along the optical indicatrix axes under lasing conditions. For X , Y -cut (light polarization $E \parallel X$) Z -cut ($E \parallel X$) crystals, the thermal lens is positive due to the large thermal expansion coefficient of the YCOB host and the strong photo-elastic effect. The latter enables efficient microchip laser operation with X -, Y -, and Z -cut Yb:YCOB crystals. The Z -cut is considered to be optimum for power scaling of Yb:YCOB microchips as it possesses a relatively weak thermal lens (sensitivity factor: $M_{Z-X} = 2.4$ and $M_{Z-Y} = 2.8 \text{ m}^{-1}/\text{W}$) with a low astigmatism degree ($S/M = 14\%$) and coexistence of two polarization states is not expected. With a 3-mm-long Z -cut Yb:YCOB microchip, 5.02 W of linearly polarized output ($E \parallel X$) is generated at 1035, . . . , 1045 nm with a slope efficiency η of 79%.

A preliminary power scaling experiment exceeding 8 W of output power confirms the potential of Yb:YCOB microchip lasers. However, for the Z -cut crystal, the laser performance at high pump levels ($P_{\text{abs}} > 15 \text{ W}$) was limited by the thermo-optic effects with the optical-to-optical efficiency clamped to $\eta_{\text{opt}} < 64\%$. Further power scaling of Yb:YCOB microchips is possible when using the so-called athermal crystal orientations with a weak, positive and nearly spherical thermal lens. This has been recently predicted for oxoborate crystals [24]. For YCOB in particular, the athermal directions lie in the $X - Y$ plane ($X \pm 62.6^\circ$) providing access to the high-gain $E \parallel Z$ polarization. Yb:YCOB microchips cut along the phase-matching directions in the $X - Y$ plane ($X \pm 46^\circ$) for self-frequency doubling are also promising for the development of CW green lasers.

References

- [1] F. Mougel, K. Dardenne, G. Aka, A. Kahn-Harari, and D. Vivien, "Ytterbium-doped $\text{Ca}_4\text{GdO}(\text{BO}_3)_3$: An efficient infrared laser and self-frequency doubling crystal," *J. Opt. Soc. Amer. B*, vol. 16, pp. 164–172, 1999.
- [2] A. Aron *et al.*, "Spectroscopic properties and laser performances of Yb:YCOB and potential of the Yb:LaCOB material," *Opt. Mater.*, vol. 16, no. 1/2, pp. 181–188, Feb./Mar. 2001.
- [3] L. Shah *et al.*, "Laser tunability in $\text{Yb}^{3+}:\text{YCa}_4\text{O}(\text{BO}_3)_3$ {Yb:YCOB}," *Opt. Commun.*, vol. 167, pp. 149–153, 1999.
- [4] H. Zhang *et al.*, "Slope efficiency of up to 73% for Yb:Ca₄YO(BO₃)₃ crystal laser pumped by a laser diode," *Appl. Phys. B*, vol. 68, pp. 1147–1149, 1999.
- [5] F. Druon *et al.*, "Efficient, tunable, zero-line diode-pumped, continuous-wave $\text{Yb}^{3+}:\text{Ca}_4\text{LnO}(\text{BO}_3)_3$ ($\text{Ln} = \text{Gd}, \text{Y}$) lasers at room temperature and application to miniature lasers," *J. Opt. Soc. Amer. B*, vol. 17, no. 1, pp. 18–22, 2000.
- [6] H. Jiang *et al.*, "Spectral and luminescent properties of Yb^{3+} ions in $\text{YCa}_4\text{O}(\text{BO}_3)_3$ crystal," *Chem. Phys. Lett.*, vol. 361, no. 5/6, pp. 499–503, Aug. 2002.
- [7] Q. Ye and B. H. T. Chai, "Crystal growth of $\text{YCa}_4\text{O}(\text{BO}_3)_3$ and its orientation," *J. Cryst. Growth*, vol. 197, pp. 228–235, 1999.
- [8] F. Mougel, A. Kahn-Harari, G. Aka, and D. Pelenc, "Structural and thermal stability of Czochralski grown GdCOB oxoborate single crystals," *J. Mater. Chem.*, vol. 8, pp. 1619–1623, 1998.
- [9] M. Iwai, T. Kobayashi, H. Furuya, Y. Mori, and T. Sasaki, "Crystal growth and optical characterization of Rare-earth (Re) calcium oxyborate $\text{ReCa}_4\text{O}(\text{BO}_3)_3$ ($\text{Re} = \text{Y}$ or Gd) as new nonlinear optical material," *Jpn. J. Appl. Phys.*, vol. 36, pp. L276–L279, 1997.
- [10] J. Liu, W. Han, H. Zhang, J. Wang, and V. Petrov, "Comparison of laser performance of Yb:YCa₄O(BO₃)₃ crystals cut along the principal optical axes," *Appl. Phys. B*, vol. 91, no. 2, pp. 329–332, May 2008.
- [11] J. Liu, H. Zhang, J. Wang, and V. Petrov, "Output-coupling-dependent polarization state of a continuous-wave Yb:YCa₄O(BO₃)₃ laser," *Opt. Lett.*, vol. 32, no. 20, pp. 2909–2911, Oct. 2007.
- [12] J. Liu, Q. Dai, Y. Wan, W. Han, and X. Tian, "The potential of Yb:YCa₄O(BO₃)₃ crystal in generating high-energy laser pulses," *Opt. Exp.*, vol. 21, no. 8, pp. 9365–9376, Apr. 2013.
- [13] H. C. Liang *et al.*, "Passively Q-switched $\text{Yb}^{3+}:\text{YCa}_4\text{O}(\text{BO}_3)_3$ laser with InGaAs quantum wells as saturable absorbers," *Appl. Opt.*, vol. 46, pp. 2292–2296, 2007.
- [14] F. Druon *et al.*, "Generation of 90-fs pulses from a mode-locked diode-pumped $\text{Yb}^{3+}:\text{Ca}_4\text{GdO}(\text{BO}_3)_3$ laser," *Opt. Lett.*, vol. 25, no. 6, pp. 423–425, Mar. 2000.
- [15] A. Yoshida *et al.*, "Diode-pumped mode-locked Yb:YCOB laser generating 35 fs pulses," *Opt. Lett.*, vol. 36, no. 22, pp. 4425–4427, 2011.
- [16] O. H. Heckl *et al.*, "Continuous-wave and modelocked Yb:YCOB thin disk laser: First demonstration and future prospects," *Opt. Exp.*, vol. 18, no. 18, pp. 19201–19208, 2010.
- [17] G. Aka *et al.*, "Linear- and nonlinear-optical properties of a new gadolinium calcium oxoborate crystal, $\text{Ca}_4\text{GdO}(\text{BO}_3)_3$," *J. Opt. Soc. Amer. B*, vol. 14, no. 9, pp. 2238–2247, 1997.
- [18] P. Segonds *et al.*, "Optical characterizations of $\text{YCa}_4\text{O}(\text{BO}_3)_3$ and $\text{Nd}:\text{YCa}_4\text{O}(\text{BO}_3)_3$ crystals," *Opt. Mater.*, vol. 29, pp. 975–982, 2007.

- [19] J. E. Hellström *et al.*, "Laser performance of Yb:GdCa₄O(BO₃)₃ compared to Yb:KGd(WO₄)₂ under diode-bar pumping," *Laser Phys.*, vol. 17, no. 10, pp. 1204–1208, Sep. 2007.
- [20] Z. M. Liao, I. Jovanovic, C. A. Ebbers, Y. Fei, and B. Chai, "Energy and average power scalable optical parametric chirped-pulse amplification in yttrium calcium oxyborate," *Opt. Lett.*, vol. 31, no. 9, pp. 1277–1279, May 2006.
- [21] J. J. Zayhowski, "Microchip lasers," *Opt. Mater.*, vol. 11, pp. 255–267, 1999.
- [22] J. M. Serres *et al.*, "Diode-pumped microchip Tm:KLu(WO₄)₂ laser with more than 3 W of output power," *Opt. Lett.*, vol. 39, no. 14, pp. 4247–4250, Jul. 2014.
- [23] S. Chénais *et al.*, "Thermal lensing measurements in diode-pumped Yb-doped GdCOB, YCOB, YSO, YAG and KGW," *Opt. Mater.*, vol. 22, no. 2, pp. 129–137, Apr. 2003.
- [24] S. A. Payne, L. L. Chase, L. K. Smith, W. L. Kway, and W. F. Krupke, "Infrared cross-section measurements for crystals doped with Er³⁺, Tm³⁺, and Ho³⁺," *IEEE J. Quantum Electron.*, vol. 28, no. 11, pp. 2619–2630, Nov. 1992.
- [25] *Lasers and Laser-Related Equipment—Test Methods for Laser Beam Widths, Divergence Angles and Beam Propagation Ratios—Part 1: Stigmatic and Simple Astigmatic Beams*, ISO 11146-1, 2005.
- [26] P. A. Loiko *et al.*, "Anisotropy of the photo-elastic effect in Nd:KGd(WO₄)₂ laser crystals," *Laser Phys. Lett.*, vol. 11, pp. 1–7, 2014.
- [27] P. Loiko *et al.*, "Thermo-optic dispersion formulas for YCOB and GdCOB laser host crystals," *Opt. Mater. Exp.*, vol. 5, pp. 1089–1097, 2015.
- [28] P. Loiko, F. Druon, P. Georges, B. Viana, and K. Yumashev, "Thermo-optic characterization of Yb:CaGdAlO₄ laser crystal," *Opt. Mater. Exp.*, vol. 4, pp. 2241–2249, 2014.
- [29] S. Chenais, F. Druon, S. Forget, F. Balembois, and P. Georges, "On thermal effects in solid-state lasers: The case of ytterbium-doped materials," *Progr. Quantum Electron.*, vol. 30, pp. 89–153, 2006.
- [30] K. Yumashev and P. Loiko, "Thermal lensing in diode-pumped [001]-cut tetragonal crystals," *Opt. Commun.*, vol. 355, pp. 543–550, Nov. 2015.
- [31] H. Shimizu, T. Nishida, H. Takeda, and T. Shiosaki, "Dielectric, elastic and piezoelectric properties of RCa₄O(BO₃)₃ (R—Rare-earth elements) crystals with monoclinic structure of point group *m*," *J. Cryst. Growth*, vol. 311, pp. 916–920, 2009.
- [32] J. Luo *et al.*, "Thermal and nonlinear optical properties of Ca₄YO(BO₃)₃," *Cryst. Res. Technol.*, vol. 36, no. 11, pp. 1215–1221, Nov. 2001.
- [33] J. M. Serres *et al.*, "Microchip laser operation of Yb-doped gallium garnets," *Opt. Mater. Exp.*, vol. 6, pp. 46–57, 2016.
- [34] P. A. Loiko *et al.*, "Thermal-lens-driven effects in N_g-cut Yb- and Tm-doped monoclinic KLu(WO₄)₂ crystals," *IEEE J. Quantum Electron.*, vol. 50, no. 8, pp. 669–676, Aug. 2014.
- [35] G. Aka *et al.*, "Ca₄REO(BO₃)₃ crystals for green and blue microchip laser generation: From crystal growth to laser and nonlinear optical properties," *Opt. Mater.*, vol. 26, no. 4, pp. 431–436, Sep. 2004.
- [36] G. Lucas-Leclin *et al.*, "Diode-pumped self-frequency-doubling Nd:GdCa₄O(BO₃)₃ lasers: Toward green microchip lasers," *J. Opt. Soc. Amer. B*, vol. 17, pp. 1526–1530, 2000.
- [37] P. Burns *et al.*, "CW diode-pumped microlaser operation at 1.5–1.6 μm in Er,Yb:YCOB," *IEEE Photon. Technol. Lett.*, vol. 14, no. 12, pp. 1677–1679, Dec. 2002.
- [38] J. M. Serres *et al.*, "Prospects of monoclinic Yb:KLu(WO₄)₂ crystal for multi-watt microchip lasers," *Opt. Mater. Exp.*, vol. 5, pp. 661–667, 2015.